Nanoscale

Plasmonic Nanoscale Temperature Shaping on a Single Titanium Nitride Nanostructure

Journal:	*Nanoscale*
Manuscript ID	NR-ART-05-2022-002442.R2
Article Type:	Paper
Date Submitted by the Author:	10-Jul-2022
Complete List of Authors:	Tamura, Mamoru; Osaka Prefecture University, Iida, Takuya; Osaka Prefecture University, Setoura, Kenji; Kobe City College of Technology, Department of Mechanical Engineering;

ARTICLE

Plasmonic Nanoscale Temperature Shaping on a Single Titanium Nitride Nanostructure

Received 00th January 20xx,
Accepted 00th January 20xx

DOI: 10.1039/x0xx00000x

Mamoru Tamura, [a, b] Takuya Iida [a, c] and Kenji Setoura [*d]

Arbitrary shaping of temperature fields at the nanometre scale is an important goal in nanotechnology; however, this is challenging because of the diffusive nature of heat transfer. In the present work, we numerically demonstrated that spatial shaping of nanoscale temperature fields can be achieved by plasmonic heating of a single titanium nitride (TiN) nanostructure. A key feature of TiN is its low thermal conductivity (k_{TiN} = 29 [W $m^{-1}K^{-1}$]) compared with ordinary plasmonic metals such as Au (k_{Au} = 314 [W $m^{-1}K^{-1}$]). When the localised surface plasmon resonance of a metal nanostructure is excited, the light intensity is converted to heat power density in the nanostructure via the Joule heating effect. For a gold nanoparticle, non-uniform spatial distributions of the heat power density will disappear because of the high thermal conductivity of Au; the nanoparticle surface will be entirely isothermal. In contrast, the spatial distributions of the heat power density can be clearly transcribed into temperature fields on a TiN nanostructure because the heat dissipation is suppressed. In fact, we revealed that highly localised temperature distributions can be selectively controlled around the TiN nanostructure at a spatial resolution of several tens of nanometres depending on the excitation wavelength. The present results indicate that arbitrary temperature shaping at the nanometre scale can be achieved by designing the heat power density in TiN nanostructures for plasmonic heating, leading to unconventional thermofluidics and thermal chemical biology.

Introduction

The term *thermoplasmonics* represents a methodology or research field that deals with the photothermal conversion of plasmonic nanoparticles. In the late 1990s, gold nanoparticles (Au NPs) were found to be nanoscale heat sources under photo-illumination.[1] Since then, a large number of applications of plasmonic heating have been proposed, including photothermal therapy,[2,3] catalysis,[4] nanofabrication,[5] nanobubble generation,[6,7] thermophoresis,[8,9] and so forth. In the 2010s, the physical description of plasmonic heating was almost accomplished by Baffou et al.[10] Nowadays, the term *thermoplasmonics* is widely accepted in the field of nanotechnology.[11] In short, major advantages of the plasmonic heating are the following two: i) highly efficient energy conversion from light to heat because of localised surface plasmon resonance (LSPR) and ii) NPs can be handled as ideal point heat sources owing to their small sizes. On the other hand, *plasmonics* dealing with LSPR or surface plasmon polaritons (SPP) have a wider range of applications in the field of nanotechnology than *thermoplasmonics*.[12–15] What makes the difference between *plasmanics* and *thermoplasmonics*? This can be ascribed to the wave nature of light and the diffusive nature of heat. The optical near field can be easily designed by changing the shape and size of the metallic nanostructures. In contrast, spatial shaping of the temperature field at the nanometre scale is difficult because of the diffusive nature of heat transfer; whether the shape of the Au nanostructure is spherical or rod, the temperature distribution would not be much different because it acts as a point heat source at the sub-micrometre scale.

To overcome such limitations and design a temperature field at the nanometre scale, we conceived the idea of using titanium nitride (TiN) instead of Au. In recent years, refractory plasmonics using transition metal nitrides such as TiN and zirconium nitride (ZrN) have attracted much attention[16–19]; these materials are suitable for applications operating at high temperatures because of their extremely high melting points (T_m ~ 3200 K).[20,21] On the other hand, the most important feature of TiN in the present work is its low thermal conductivity compared with Au: k_{TiN} = 29 [W $m^{-1}K^{-1}$][22] and k_{Au} = 314 [W $m^{-1}K^{-1}$][23], respectively. In the following section, we explain why TiN is beneficial for nanoscale temperature shaping. Upon continuous excitation of the LSPR of a metallic NP, the light intensity is converted to heat power density via the Joule heating effect (Scheme 1a and b).[24] Then, the NP releases heat, which creates a static temperature increase around the NP. In general, the NP surface is believed to be isothermal under illumination.[25] In actuality, the surface temperature in Scheme 1c is slightly nonuniform because spatial patterns of the heat

[a.] *Research Institute for Light-induced Acceleration System (RILACS), Osaka Metropolitan University, Sakai, Osaka 599-8570, Japan*
[b.] *Division of Materials Physics, Graduate School of Engineering Science, Osaka University, Toyonaka, Osaka, 560-8531, Japan*
[c.] *Department of Physics, Osaka Metropolitan University, Sakai, Osaka 599-8531, Japan*
[d.] *Department of Mechanical Engineering, Kobe City College of Technology, Kobe, Hyogo 651-2194, Japan. E-mail: setoura@kobe-kosen.ac.jp*
† Electronic Supplementary Information (ESI) available: [details of any supplementary information available should be included here]. See DOI: 10.1039/x0xx00000x

power density are reflected in the temperature field. However, the non-uniform patterns of the heat power density disappear owing to the high thermal conductivity of Au, resulting in an almost isothermal surface temperature (Scheme 1c). Therefore, we presumed that the heat power density would be transcribed into the temperature field on the TiN nanostructure because the heat dissipation can be suppressed (Scheme 1d).

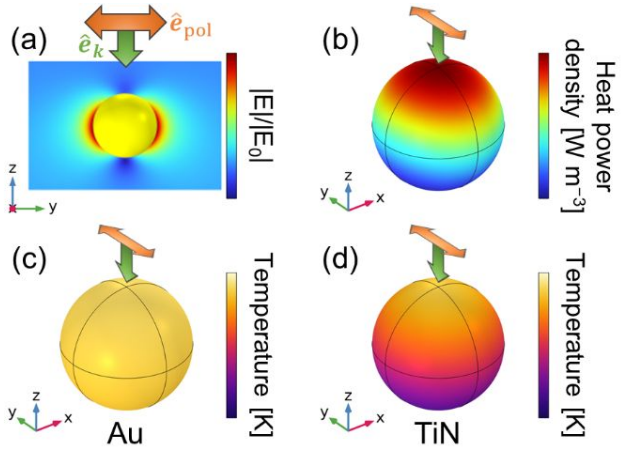

Scheme 1. (a) Electric field around a plasmonic nanoparticle under illumination of linearly polarized light. (b) Heat power density calculated from (a) on the basis of the Joule heating effect. (c) Surface temperature of a Au nanoparticle under illumination. (d) Surface temperature of a TiN nanoparticle under illumination.

To demonstrate this idea, we performed numerical simulations of plasmonic heating of a TiN nanoring. As a result, we found that the temperature distribution around the TiN nanorings changed drastically depending on the excitation wavelength under the illumination of a linearly polarised plane wave, because the spatial patterns of the heat power density strongly depend on the excitation wavelength. In other words, nanoscale temperature shaping can be achieved by designing the shape of the nanostructures and the parameters of the incident light. The present method will be of great use in the development of new applications in thermoplasmonics.

Results and discussion

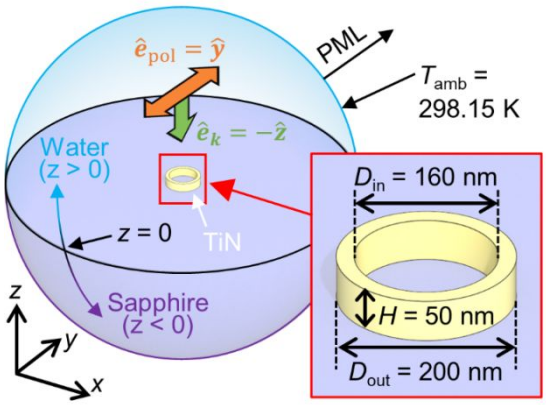

Fig. 1. Simulation model.

In general, dynamics of the plasmonic heating can be divided into the following three steps[26–28]: i) electronic excitation and subsequent thermalisation followed by heat generation in the nanoparticle in the time region from femtosecond to a few picoseconds. ii) heat diffusion from the nanoparticle to a surrounding medium in the time region from picosecond to nanosecond. iii) when a continuous light source employed, temperatures of the nanoparticle and the surrounding medium reaches steady-state within a few hundreds of nanoseconds[25]. In this work, we only deal with the steady-state heat conduction, because we focused on the static temperature distributions around the nanoparticle. Fig. 1 shows the geometry of the numerical simulation. The three-dimensional spherical system was filled with water ($z > 0$) and a sapphire substrate ($z < 0$). TiN nanorings with an outer diameter D_{out} = 200 nm, inner diameter D_{in} = 160 nm, and height H = 50 nm were placed on the substrate. We assumed the injection of a y-polarised plane wave in the −z-direction. Using the finite element method in COMSOL Multiphysics (version 6.0), we solved Maxwell's equations in the frequency domain and steady-state heat conduction as follows:

$$\nabla \times \nabla \times \mathbf{E}(\mathbf{r},\omega) = \frac{\omega^2}{c^2}\varepsilon(\mathbf{r},\omega)\mathbf{E}(\mathbf{r},\omega), \quad (1)$$

$$\nabla \cdot [k(\mathbf{r})\nabla T(\mathbf{r})] = -q_e(\mathbf{r},\omega). \quad (2)$$

Here, **E** is the electric field, ω is the angular frequency of light, c is the speed of light, ε is the relative dielectric function, k is the thermal conductivity, T is the temperature, q_e is the volumetric heat power density owing to the Joule heating effect. The Joule heating effect of an oscillating electromagnetic field at an arbitrary frequency is expressed as follows,[29,30]

$$q_e(\mathbf{r},\omega) = \frac{\omega}{2}\varepsilon_0 \,\mathrm{Im}[\varepsilon(\mathbf{r},\omega)]|\mathbf{E}(\mathbf{r},\omega)|^2, \quad (3)$$

where ε_0 is vacuum permittivity. As boundary conditions, the simulation system was surrounded by perfectly matched layers (PMLs) for Eqs. (1), and a Dirichlet boundary condition with $T(r$ = 1μm) = T_{amb} = 298.15 K was imposed for Eq. (2). In addition, we characterised the scattering and absorption cross sections of the TiN nanorings by integrating their scattering field and electromagnetic heating as follows:

$$\sigma_{scat}(\omega) = \frac{1}{I_{in}}\iint_{NR}(\mathbf{n}\cdot\mathbf{S}_{scat})\,dS, \quad (4)$$

$$\sigma_{abs}(\omega) = \frac{1}{I_{in}}\iiint_{NR} q_e(\mathbf{r},\omega)\,dV, \quad (5)$$

where integration was carried out over the nanoring surface and volume, I_{in} is the incident intensity, and **n** is the normal

vector pointing to the outward nanoring. $\mathbf{S}_{scat}$ is the Poynting vector of the scattered field solved using Eq. (1) with an incident field as a solution of the water/substrate system without nanorings. When carrying out the simulation, the symmetry of the structure was used to reduce the calculation costs. The material properties are summarised in Table 1. The previously reported value of the relative complex dielectric function was used for $\varepsilon_{TiN}(\omega)$ described by the Drude model.[31,32] The sapphire substrate was chosen to enhance the temperature gradients [K m^{-1}] around the TiN nanorings owing to its high thermal conductivity.[33,34] For comparison, regarding thermal conductivity, the gold property was also used.

Table 1. Material properties.

	Water	Sapphire	TiN	Au
Relative dielectric function ε	1.33[2]	1.77[2]	$\varepsilon_{TiN}(\omega)$	-
Thermal conductivity k [W $m^{-1}K^{-1}$]	0.6	42	29	314

Fig. 2 shows the calculated absorption and scattering cross-sections of the TiN nanorings evaluated using Eqs. (4) and (5), respectively. In the absorption spectrum, one can clearly see an LSPR peak arising from the dipolar mode at a wavelength of approximately 1900 nm. As will be shown later, excitation of the TiN nanoring at this LSPR peak led to a highly nonuniform temperature distribution, whereas the nanoring surface was almost isothermal upon off-resonant excitation at a wavelength of 500 nm.

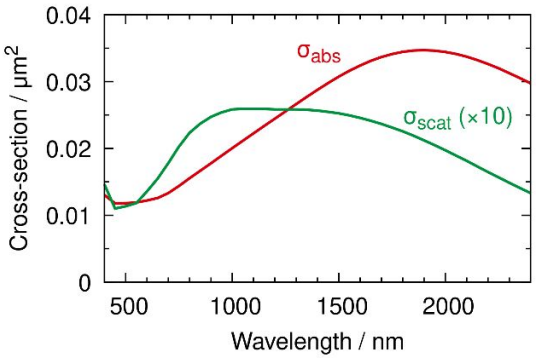

Fig. 2. Absorption and scattering cross-sections of the TiN nanoring.

Fig. 3 shows the spatial distributions of the electric field, integrated heat power density, and temperature. The upper and lower panels represent the numerical results at excitation wavelengths of 500 and 1900 nm, respectively. Note that the result in Figs. 3b and e differ from the *volumetric* heat power density in Eq. (3); it is integrated in the z-direction. At both wavelengths, similar optical near-fields were obtained around the nanoring, as shown in Fig. 3a and –d; these spatial distributions can be ascribed to the dipolar mode of LSPR along the y-axis. However, the heat power density around the middle of the nanoring in Fig. 3e was much greater than that in Fig. 3b; the maximum value of integration was larger than the incident intensity I_{in} = 1 MW cm^{-2}. The temperature fields were calculated from the heat power densities, as shown in Fig. 3c and -f. At an excitation wavelength of 500 nm, the nanoring surface was almost isothermal because the heat source in Fig. 3b exhibited a small nonuniformity. In contrast, surprisingly, the temperature distribution was highly nonuniform at an

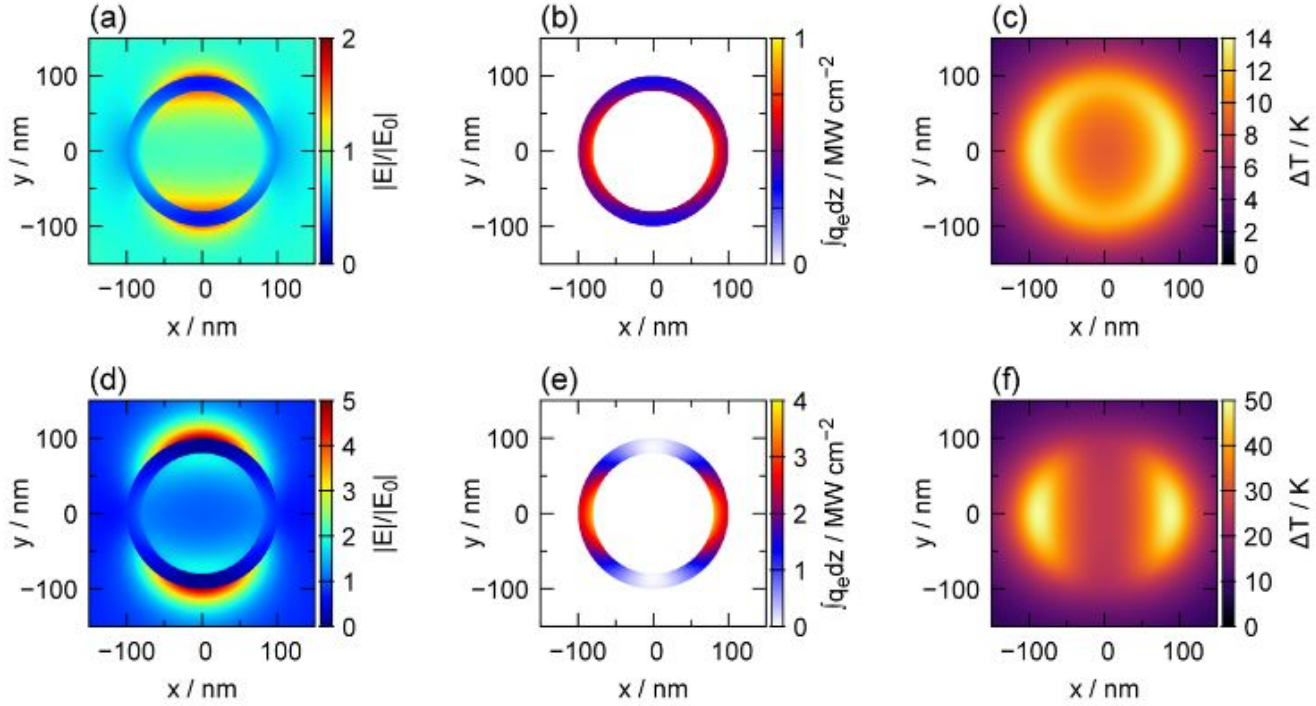

Fig. 3. (a)(d) Electric field amplitude normalized by the incident one $|\mathbf{E}_0|$ at z = 25 nm. (b)(e) Heat power density integrated over z direction. (c)(f) Temperature rise $\Delta T(\mathbf{r}) = T(\mathbf{r}) - T_{amb}$ at z = 60 nm. The excitation wavelengths were λ = 500 nm for (a)(b)(c) and λ = 1900 nm for (d)(e)(f), respectively. Here, an incident light intensity was set to I_0 = 1 MW/cm².

excitation wavelength of 1900 nm, as shown in Fig. 3f, indicating that the temperature field inherited the spatial patterns of the heat power density.

To clarify that the origin of the nonuniform temperature field in Fig. 3f is the thermal conductivity of TiN, we carried out numerical simulations in the same manner as before using the thermal conductivity of Au for the nanoring, instead of TiN; please see the results shown in Fig. S1 in the Electronic Supplementary Information (ESI). At excitation wavelengths of 500 and 1900 nm, the temperatures on the nanoring surface were almost isothermal. These results strongly indicate that the low thermal conductivity of TiN permitted nanoscale temperature shaping around the plasmonic nanostructure.

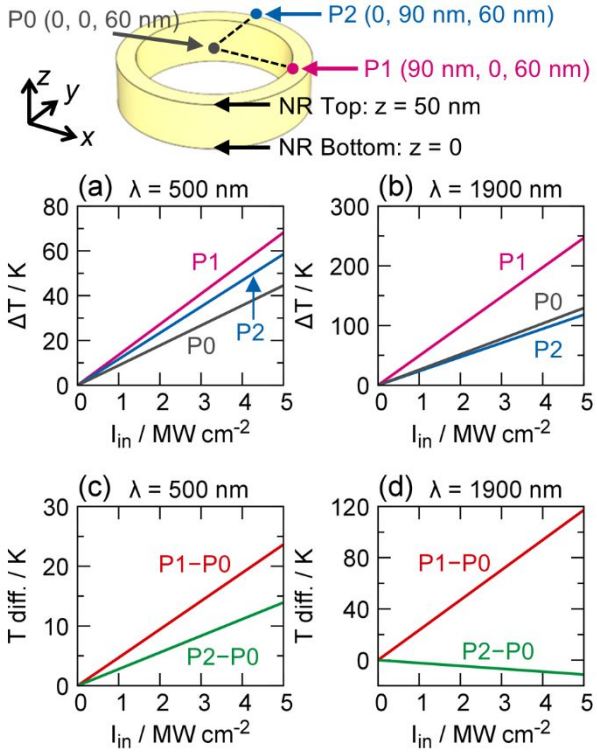

Fig. 4. Temperature increase at specific locations around the TiN nanoring as a function of light intensity. (a)(b) Temperature increase $\Delta T(\mathbf{r}) = T(\mathbf{r}) - T_{amb}$ at the location $\mathbf{r}$ = P0, P1, and P2. (c)(d) Temperature difference from T(r = P0) to T(r = P1) and T(r=P2). Excitation wavelengths were (a)(c) 500 nm and (c)(d) 1900 nm, respectively.

To gain a deeper insight into the results in Fig. 3, we performed additional calculations on the temperature increase as a function of the incident light intensity, as shown in Fig. 4. As shown in the upper diagram (a schematic representation of the TiN nanoring) in Fig. 4, these temperatures were probed at P0, P1, and P2. The temperature increased linearly with the incident intensity I_{in} for all points. As shown in Fig. 4a, at an excitation wavelength of 500 nm, the temperature increase at P1 exhibited a slope similar to that of P2. In contrast, at an excitation wavelength of 1900 nm, the slope of the temperature increase at P1 was almost twice that at P2 (Fig. 4b).

To visualise the difference between the excitation wavelengths of 500 and 1900 nm, we plotted the temperature differences (Tdiff. [K]) as a function of the incident light intensity, as shown in Fig. 4c and d; T diff. was obtained by subtracting the temperature at P0 from those at P1 and P2. In Fig. 4c, the both T diff. linearly increases with I_{in}; this is an ordinary dependence on the input power in steady-state heat conduction. In contrast, the difference between the two linear curves in Fig. 4d increases as a function of I_{in} because of the negative slope of (P2 – P0). This result implies a great possibility of temperature shaping with TiN, because the temperature difference at the nanometre scale can be more pronounced by simply increasing the light intensity. This surprising behaviour in Fig. 4d cannot be confirmed when the thermal conductivity of Au is employed for the nanoring, as shown in ESI Fig. S2. In addition, we performed numerical calculations of the temperature increase at P1, P2 and P0 as a function of the thermal conductivity of the nanoring: i.e. the value of the thermal conductivity was swept over a range from k_{water} = 0.6 [W m^{-1}K^{-1}] to k_{Au} = 314 [W m^{-1}K^{-1}]. The result is shown in ESI as Figure S3. It has been clearly demonstrated that the nanoscale temperature shaping is accomplished by the low thermal conductivity of TiN.

Temperature shaping using TiN nanostructures is promising for various applications in thermoplasmonics. By choosing the excitation wavelength, we can switch the mode of the temperature distribution to whole heating or local heating on the nanoring surface. In addition, the local heating mode shown in Fig. 3f can be rotated by rotating the polarisation of the incident light. These features will assist further development of photothermal manipulation methods for small objects based on fluid convection[35–39] (natural and Marangoni convection) and thermophoresis[40–42]. For these applications, one can use 2D periodic arrays of the TiN nanostructures. In actuality, the entire temperature distribution on the 2D array can be divided into the following two regimes depending on both the interparticle distance and the size of the illuminated system[43]: i) a localised regime and ii) a delocalised regime. In our case, the former is desired because the individual nanostructures should act as isolated nanoheaters. For this purpose, the individual nanostructures should be well separated and the illuminated area should be reduced. Even if the interparticle distance is large enough, the entire temperature distribution can be delocalised when the total size of the illuminated array is large[43].

Before going to conclusions, we mention outlook of this method, the site-selective plasmonic nanoheater. First, to improve spatial resolution of the nanoscale temperature shaping, one can use manganese (Mn) as a plasmonic material. A thermal conductivity of Mn is 7.8 W m^{-1}K^{-1}.[23] This value is only about 27 % compared with that of TiN, therefore, the spatial resolution of the nanoscale temperature shaping will be improved. However, there has been only a few papers reporting on fabrication of Mn nanoparticles[44], indicating that the fabrication methods of the plasmonic Mn nanostructures are still under development. Therefore, we employed TiN as the plasmonic material to propose the realistic nanosystem in this paper. Second, it might be possible to transcribe high ordered plasmonic modes such as a quadrupole mode into nanoscale temperature fields, although the quadrupole modes have smaller spatial structures compared with those of the dipolar modes; this will further add the tunability on the plasmonic

nanoscale temperature shaping. Third is why we chose the ring shape in this work. This is because the heat power density can be confined in the narrower regions compared to that in the nanodisk at a same outer diameter. For the same reason, core-shell nanoparticles (silica core and metal outer shell) will be interesting compared to pure metal nanospheres. On the other hand, we expect that nanorods with high aspect ratios will be of particular interest because various plasmonic modes can be excited depending on the irradiation conditions, resulting in localisation of the heat dissipation in well-defined regions.

Conclusions

We clarified the possibility of nanoscale temperature shaping of TiN nanostructures in plasmonic heating. Using the finite-element method, we performed numerical simulations based on electromagnetism and heat conduction. First, the electric fields created by the LSPR of TiN nanorings were calculated. Second, the heat power density of the TiN nanorings was obtained from the electric fields based on the Joule heating effect. Finally, temperature distributions around the TiN nanoring were calculated; the nanoscale temperature field was highly nonuniform at an excitation wavelength of 1900 nm, while the nanoring surface was almost isothermal under illumination at 500 nm. These results strongly indicate that the temperature field can inherit the spatial patterns of the heat power density when a plasmonic material with a low thermal conductivity is employed because heat dissipation is suppressed. It has been revealed that the nanoscale temperature field can be modulated by changing parameters of incident light, such as wavelength, polarization, and so forth. In other words, nanoscale temperature shaping can be achieved via plasmonic Joule heating by designing the heat power density. The present method will pave the way for broader applications in site-selective plasmonic nanoheaters related to molecular thermofluidics, thermal chemistry, and molecular biology.

Author Contributions

K.S. coordinated the project. M.T., T.I., and K.S. performed numerical calculations. The manuscript was written through the contributions of all authors. All the authors approved the final version of the manuscript.

Conflicts of interest

There are no conflicts to declare.

Acknowledgements

This work was supported by JSPS KAKENHI Grant Numbers JP20H02075, JP20K15196, JP21H04964, JP21H01785, and JP20K20541, and JST-Mirai Program Grant Numbers JPMJMI18GA and JPMJMI21G1. The authors thank Prof. H. Ishihara for his kind support. The authors thank Editage (www.editage.com) for English language editing.

Notes and references

1 H. Inouye, K. Tanaka, I. Tanahashi and K. Hirao, *Phys. Rev. B*, 1998, **57**, 11334–11340.

2 E. C. Dreaden, A. M. Alkilany, X. Huang, C. J. Murphy and M. A. El-Sayed, *Chem. Soc. Rev.*, 2012, **41**, 2740–2779.

3 L. Jauffred, A. Samadi, H. Klingberg, P. M. Bendix and L. B. Oddershede, *Chem. Rev.*, 2019, **119**, 8087–8130.

4 Y. Dubi, I. W. Un and Y. Sivan, *Chem. Sci.*, 2020, **11**, 5017–5027.

5 A. S. Urban, S. Carretero-Palacios, A. A. Lutich, T. Lohmüller, J. Feldmann and F. Jäckel, *Nanoscale*, 2014, **6**, 4458–74.

6 G. Baffou, J. Polleux, H. Rigneault and S. Monneret, *J. Phys. Chem. C*, 2014, **118**, 4890–4898.

7 M. Li, T. Lohmüller and J. Feldmann, *Nano Lett.*, 2015, **15**, 770–5.

8 A. P. Bregulla, A. Würger, K. Günther, M. Mertig and F. Cichos, *Phys. Rev. Lett.*, 2016, **116**, 188303.

9 L. Lin, M. Wang, X. Peng, E. N. Lissek, Z. Mao, L. Scarabelli, E. Adkins, S. Coskun, H. E. Unalan, B. A. Korgel, L. M. Liz-Marzán, E.-L. Florin and Y. Zheng, *Nat. Photonics*, 2018, **12**, 195–201.

10 G. Baffou and R. Quidant, *Laser Photon. Rev.*, 2013, **7**, 171–187.

11 G. Baffou, F. Cichos and R. Quidant, *Nat. Mater.*, 2020, **19**, 946–958.

12 S. A. Maier and H. A. Atwater, *J. Appl. Phys.*, 2005, **98**, 011101.

13 E. Ozbay, *Science (80-.).*, 2006, **311**, 189–193.

14 J. A. Schuller, E. S. Barnard, W. Cai, Y. C. Jun, J. S. White and M. L. Brongersma, *Nat. Mater.*, 2010, **9**, 193–204.

15 T. Iida, *J. Phys. Chem. Lett.*, 2012, **3**, 332–336.

16 A. Lalisse, G. Tessier, J. Plain and G. Baffou, *J. Phys. Chem. C*, 2015, **119**, 25518–25528.

17 A. Lalisse, G. Tessier, J. Plain and G. Baffou, *Sci. Rep.*, 2016, **6**, 38647.

18 U. Guler, J. C. Ndukaife, G. V. Naik, A. G. A. Nnanna, A. V. Kildishev, V. M. Shalaev and A. Boltasseva, *Nano Lett.*, 2013, **13**, 6078–6083.

19 U. Guler, V. M. Shalaev and A. Boltasseva, *Mater. Today*, 2015, **18**, 227–237.

20 S. Ishii, R. Kamakura, H. Sakamoto, T. D. Dao, S. L. Shinde, T. Nagao, K. Fujita, K. Namura, M. Suzuki, S. Murai and K. Tanaka, *Nanoscale*, 2018, **10**, 18451–18456.

21 K. Setoura and S. Ito, *AIP Adcanves*, 2021, **11**, 115027.

22 W. Lengauer, S. Binder, K. Aigner, P. Ettmayer, A. Guillou, J. Debuigne and G. Groboth, *J. Alloys Compd.*, 1995, **217**, 137–147.

23 Y. Touloukian, Ed., *Thermophysical Properties of Matter - The TPRC Data Series. Volume 1. Thermal Conductivity - Metallic Elements and Alloys*, Plenum Press, New York, 1970.

24 G. Baffou, R. Quidant and C. Girard, *Appl. Phys. Lett.*, 2009, **94**, 153109.

25 P. Keblinski, D. G. Cahill, A. Bodapati, C. R. Sullivan and T. A. Taton, *J. Appl. Phys.*, 2006, **100**, 054305.

26 G. V Hartland, *Chem. Rev.*, 2011, **111**, 3858–3887.

27 A. Siems, S. A. L. Weber, J. Boneberg and A. Plech, *New J. Phys.*, 2011, **13**, 043018.

28 G. Baffou and H. Rigneault, *Phys. Rev. B - Condens. Matter Mater. Phys.*, 2011, **84**, 035415.

29 C. Kojima, Y. Watanabe, H. Hattori and T. Iida, *J. Phys. Chem. C*, 2011, **115**, 19091–19095.

30 G. Baffou, *Thermoplasmonics: Heating metal nanoparticles using light*, Cambridge University Press, 2017.

31 J. Pflüger and J. Fink., in *Handbook of optical constants of solids II*, Academic Press, 1991, pp. 293–310.

32 J. Pflüger, J. Fink, W. Weber, K. P. Bohnen and G. Crecelius, *Phys. Rev. B*, 1984, **30**, 1155.

33 K. Setoura, Y. Okada, D. Werner and S. Hashimoto, *ACS Nano*, 2013, **7**, 7874–7885.

34 J. Gargiulo, T. Brick, I. L. Violi, F. C. Herrera, T. Shibanuma, P. Albella, F. G. Requejo, E. Cortés, S. A. Maier and F. D. Stefani, *Nano Lett.*, 2017, **17**, 5747–5755.

35 K. Setoura, S. Ito and H. Miyasaka, *Nanoscale*, 2017, **9**, 719–730.

36 F. Karim, E. S. Vasquez, Y. Sun and C. Zhao, *Nanoscale*, 2019, **11**, 20589–20597.

37 Y. Nishimura, K. Nishida, Y. Yamamoto, S. Ito, S. Tokonami and T. Iida, *J. Phys. Chem. C*, 2014, **118**, 18799–18804.

38 T. Iida, Y. Nishimura, M. Tamura, K. Nishida, S. Ito and S. Tokonami, *Sci. Rep.*, 2016, **6**, 1–9.

39 Y. Yamamoto, S. Tokonami and T. Iida, *ACS Appl. Bio Mater.*, 2019, **2**, 1561–1568.

40 K. Setoura, T. Tsuji, S. Ito, S. Kawano and H. Miyasaka, *Nanoscale*, 2019, **11**, 21093–21102.

41 S. Shakib, B. Rogez, S. Khadir, J. Polleux, A. Würger and G. Baffou, *J. Phys. Chem. C*, 2021, **125**, 21533–21542.

42 M. Fränzl, T. Thalheim, J. Adler, D. Huster, J. Posseckardt, M. Mertig and F. Cichos, *Nat. Methods*, 2019, **16**, 611–614.

43 G. Baffou, P. Berto, E. Bermúdez Ureña, R. Quidant, S. Monneret, J. Polleux and H. Rigneault, *ACS Nano*, 2013, **7**, 6478–6488.

44 O. A. Yeshchenko, I. M. Dmitruk, A. A. Alexeenko and A. M. Dmytruk, *Appl. Surf. Sci.*, 2008, **254**, 2736–2742.